Volcanic plume height correlated with magma pressure change at Grímsvötn volcano, Iceland

1 Supplementary Methods

1.1 Mt. Grímsfjall research station

Mt. Grímsfjall on the southern caldera rim of Grímsvötn (Fig. 1) is the only present nunatak (ice free area) with solid bedrock on the Grímsvötn volcano. Environmental conditions are extreme, especially during winter when temperatures can range from -20 to -30°C. Average annual precipitation is about 3 m (water equivalent; falls mostly as snow) and blizzards with high winds are common. Icing conditions are frequent. The location is near the middle of the Vatnajökull ice cap and to reach the station travel of 40-70 km from the ice edge is required. The Icelandic Glaciological Society, a non-profit organization supporting research and travel on glaciers in Iceland, has huts on Mt. Grímsfjall and supports research facilities there as well as expeditions to the area. The Icelandic Meteorological Office operates continuously running geophysical equipment on Mt. Grímsfjall, including a seismometer, GPS geodetic receiver, and an electronic tiltmeter. The data from the tiltmeter are digitized and transmitted along with seismic recordings. The seismic and geodetic data is transmitted continuously by a spread spectrum link to a station south of the Vatnajökull ice cap (Skeiðarársandur area). There, the data is stored on a Linux computer with network connection to the Icelandic Meteorological Office through a 3G Internet connection. Continuous data streams were uninterrupted during the Grímsvötn 2011 eruption, despite the instruments being only at 6 km distance from the base of an eruption plume reaching up to 20 km height and loaded with ash and frequent lightning.

The seismometer is a Lennartz **LE-3D/5s** with Guralp DM24 mk3 digitizer. The tiltmeter is an electronic Applied Geomechanics biaxial tiltmeter, model 711-2A(4X). It measures north-south and east-west components of tilt. The continuously recording GPS station GFUM has a Trimble NetRS instrument recording the GPS signals at a rate of 5 Hz, 1 Hz, and every15 s. The station has a Trimble Chokering antenna (TRM29659.00) with a SCIGN (Southern California Integrated GPS Network) short dome mounted on a 2 m high steel pipe, 5 inches in diameter. In order to reduce effects of extreme icing conditions, a heating coil is wound around the steel pipe, which is also sheltered inside a black high-gloss plastic pipe (45 cm inner diameter). The heat coil is connected to a methanol heat pipe getting heat from a 10 m

2

deep borehole. This has proven successful at de-icing although during some storms, ice may collect on the dome as a result of sleet freezing on it. Prior to the installation of the continuous site in 2004 intermittent GPS measurements were carried out at another benchmark (GRIM) at a distance of 206 m from the continuous site. Measurements at GRIM, still being continued at least annually, show good agreement with GFUM.

1.2 Seismicity and tremor associated with the eruption

Over 40 earthquakes, ranging in size from Ml 0.4 to Ml 3.1, occurred shortly before the onset of the Grímsvötn eruption at 19:00 UTC, 21 May 2011 (Supplementary Fig. 1). At the same time, seismic tremor at Grímsfjall increased substantially, signifying continuous, localized earthquakes. Between 18:30 and 19:00 UTC, low frequency (0.5 - 1 Hz) tremor amplified, suggestive of harmonic tremor due to magma ascent (Supplementary Fig. 1). In the six-and-a-half years preceding the 2011 eruption seismicity beneath Grímsvötn increased progressively, reaching a maximum earthquake rate immediately before the eruption began. The closest seismic station to the 2011 eruption is at Mt. Grímsfjall, located about 6 km to the east; the next stations are over 50 km away from Grímsvötn. Both the geographic arrangement of the seismic network and the selected velocity model can affect the accuracy of single-event locations. However, some changes in earthquake depth are apparent beneath Grímsvötn immediately before the 2011 eruption. Initially, earthquakes occurred at depths of 2 to 4 km, whereas in the minutes before the eruption, hypocenters clustered near to the surface at less than 1 km depth.

1.3 Volume and density of erupted tephra

The thickness of the tephra layer formed in the eruption was sampled at about 300 localities in the eastern part of Iceland, mostly in the days and weeks after the eruption ended. The majority of the sample points were located on Vatnajökull and the areas to the south of Grímsvötn where the largest part of the fallout occurred. Fallout outside Iceland is estimated using an exponential thinning model[24]. The bulk density of the tephra was measured for several locations and the average found to be about 1000 kg m^{-3}.

3

1.4 GPS data and analysis

The GPS data were analyzed with two different approaches. We estimated 8 hour solutions from 15 s data and kinematic baseline solutions from 1Hz and 5 Hz data.

8 hour strategy

The 8 hour solutions were produced to estimate the co-eruptive offset in a fixed reference frame. Data from GFUM were analyzed using GAMIT/GLOBK 10.4[21] along with 98 global CGPS stations and 59 CGPS stations within Iceland[25]. The data were analyzed using IGS05 absolute antenna phase center models, applying a cutoff angle of 10 degrees to reduce noise and multipath. We also applied the FES2004 ocean-loading model. We used 51 of the global stations to constrain the solution to the ITRF05 reference frame. The co-eruptive offset was estimated from averaging daily pre-eruption solutions from 18 to 20 May and comparing these to 8 hour solutions from 21 to 28 May. The maximum co-eruptive change was obtained mid-day on 23 May. Significant co-eruptive displacement was observed at one other CGPS station, DYNC, 43 km north of Grímsvötn. The station moved 8 ± 2 mm south towards Grímsvötn and as a result we excluded it in our kinematic analysis. Other CGPS stations had 3 mm or less co-eruptive displacement.

1 Hz strategy

As described in the main text, we obtained the 1 Hz kinematic GPS solutions using the TRACK module of the GAMIT/GLOBK software[21], reducing multi-path effects by sidereal filtering, subtracting solutions from 20 May using the most common orbit repeat time of 24 hours minus 246 seconds[22,23]. Final orbits of GPS satellites distributed by the International GNSS Service (IGS)[26] and IGS05 antenna phase center models were applied. We found that a cutoff angle of 10 degrees reduces the noise, resulting in a much cleaner solution than lower cutoff angles. Due to the generally large distances between the base stations and GFUM, as well as differences in altitude, we estimate the atmospheric delay but assume the same Ionosphere. We estimate the position of GFUM with respect to 7 other high rate GPS stations in Iceland (JOKU, FJOC, HOFN, INTA, HAUC, STKA, and AUST) with baselines ranging from 48-120 km (Fig. 1, Supplementary Fig. 2).

4

The spike we see in the north and vertical components of the final time series at GFUM (Supplementary Fig. 3) are likely multi-path residuals that we could not fully remove. The spikes occur on the days prior to the eruption at roughly the same time for all station pairs; including ones without GFUM. To dampen this effect we apply a 5 minute running average filter to the time series. However, during the time of the eruption we also see an increase in RMS misfit after the onset of the eruption, mostly in the vertical, which hints towards obstruction of satellite-station line of sight through the plume for some satellite-station pairs as observed elsewhere[27-29].
We average the resulting 7 positioning time series we got for GFUM with respect to the 7 base stations to produce the data we work with in the modeling of the data (Supplementary Fig. 4 and 5).

1.5 Tilt data and analysis

The tiltmeter on Grímsfjall is a high-gain biaxial sensor, manufactured by Applied Geomechanics Inc. (model 711-2A). The sensor is bolted via a three-pin mounting into a concrete plinth that is coupled firmly to bedrock at an elevation of 1,710 m a.s.l. Variations in tilt are detected electrically using an air bubble within a glass tube. As the sensor tilts, changes in electrical resistance occur; this signal is then converted into a measurement of the magnitude and direction of tilt. The tiltmeter is housed in a shallow wooden enclosure to reduce thermoelastic effects due to temperature changes. Although sub-freezing temperatures dominate weather conditions at Grímsfjall, geothermal heat is conducted to the nunatak, ensuring that the ambient temperature of the tiltmeter remains within the operating minimum of -25 °C. The tiltmeter has an angular range of +/-8,000 micro-radians (μrad) (+/-0.46°) and a minimum resolution of 1 μrad. The sensor is calibrated to record tilt changes to at least 3.5% accuracy without temperature compensation.

The tiltmeter is co-located with the seismic unit on Mt. Grímsfjall. The raw data streams from the tiltmeter are channeled to the Guralp DM24 mk3 digitizer for the seismic unit. The digitized tilt signals are then transmitted through available channels on the seismic unit along with seismic recordings. Two channels of different type are available, contributing to different resolution of tilt components. The north-south tilt component is available at 100 Hz with 22-bit resolution, but the east-west

5

component is only sampled at 4 Hz with a 16-bit resolution. We consider here only 5-minute averages of tilt, making the difference in original resolution not important. The data had some perturbations in the form of artificial spikes and offsets, which were corrected for during post processing, resulting from the digitization of the data. The north-south and east-west components of tilts are displayed in Supplementary Fig. 4.

The uncertainty in the tilt originates from various sources. The data was not corrected for temperature and thus we consider a 3.5% inherent uncertainty, in line with the manufacturer calibration of the tiltmeter. Earth tides were also not corrected for; we add a random error of 1 μrad to account for this but the effect is smaller over short time intervals[30,31]. We furthermore consider potential long-term drift of the instrument due to a number of factors such as temperature influence of the bedrock and mounting of the tiltmeter to the ground (thermoelastic effects). A tiltmeter placed at a depth of few meters in Iceland revealed a drift of up to 0.3 μrad/day[30], but as the Grímsvötn tiltmeter is placed at the surface (in freezing conditions though) we evaluate the potential long-term drift to be higher, or 1 μrad/day. The correction of offsets in the raw data is furthermore expected to be a source of error; with uncertainty due to each offset estimated as 1 μrad. We add up the variance associated with each of these contributions to derive the following equation for uncertainty on tilt components (5-minute averages):

$$\sigma_{tilt,x}^2 = (0.035\delta_x)^2 + (1\mu\text{rad})^2\left[1 + T^2 + N\right]$$

where δ_x is the observed component of tilt in μrad, T is the time span of the tilt change considered in days, N is the number of offset that needed correction, and $\sigma_{tilt,x}$ is the resulting uncertainty for the tilt component (north-south and east-west). Uncertainties according to this equation are listed in Supplementary Table 1. They are 4-5% of the observed change, reflecting high signal-to-noise ratio as a large tilt signal was produced over a relatively short time interval.

6

1.6 The magma chamber model and evaluation of model parameters

The source model of pressure change in a spherical volume in elastic halfspace (the so called Mogi model) is well described e.g. by Dzurisin[1] and Segall[12]. There are many underlying assumptions, the first being that magma resides as an isolated spherical body within an otherwise homogenous elastic halfspace. The radius of the sphere is also assumed to be small compared to its depth. These are oversimplification but nevertheless the model has been used widely and successfully. These assumptions are likely to affect the outcome of any modeling; uncertainties reported on model parameters reflect thus only model uncertainties, assuming the model is the correct one. By the word magma chamber we refer here to an upper crustal magma storage system.

The resulting displacement field at the surface of the Earth, according to the Mogi model[11], is radially symmetric, with center of symmetry directly above the source. The "Mogi" point source is considered a good approximation for a spherical chamber when the chamber depth is large compared to its radius[13]. The equations for vertical and horizontal displacements, and radial tilt (with all parameters explained in the main text) are:

$$u_r = C \frac{r}{\left(d^2 + r^2\right)^{3/2}} \qquad u_z = C \frac{d}{\left(d^2 + r^2\right)^{3/2}} \qquad \delta = C \frac{-3dr}{\left(d^2 + r^2\right)^{5/2}}$$

These equations assume a Poisson's ratio of 0.25. The special application of the model considered here is that tilt and displacement is measured at the same location. In that case, three observables (u_r, u_z, δ) allow the determination of the three model parameters in the equations above: r, d, and C. Inherent to these equations is that:

$$\frac{u_z}{u_r} = \frac{d}{r}$$

which shows that the three-dimensional displacement at any location on the surface of the Earth points in direction directly to or from the magma chamber. Making use of the relation:

$$\delta = \frac{-3r}{\left(d^2 + r^2\right)} u_z$$

7

combined with

$$r = \frac{u_r}{u_z} d$$

one can derive the following equation for the depth of the source:

$$d = \frac{-3u_z}{\delta} \frac{\left(u_r/u_z\right)}{1+\left(u_r/u_z\right)^2}$$

The equation for vertical displacement can be rearranged so it gives:

$$C = u_z d^2 \left(1+\left(\frac{u_r}{u_z}\right)^2\right)^{3/2}$$

Combined with the equation above for *d*, then equation (2) in the main text is derived. With these equations a direct analytical estimate for the Mogi source parameters can be derived from the observations listed in Table 1 (upper part). This we refer to as the analytical approach to derive the parameters.

For comparison with the analytical approach, we also model the surface deformation observed at GFUM with GPS and tilt (same data in Table 1), with an inversion approach. Given the sparse dataset, we model the deformation again with a single Mogi point source in an elastic half-space[11], now assuming a Poisson's ratio 0.27. We use Markov chain Monte Carlo sampling in a similar manner as Hooper *et al.*[32] to build the probability distribution of the model parameters, assuming a uniform prior probability.

The GFUM geodetic site is located at 17.26660°W and 64.40676°N. For the inversion, a center of coordinate system is defined at [-17.31234°W, 64.42922°N]. The depth estimate is relative to the geodetic station (also for the analytical approach). The inversion results in the following maximum likelihood range of model parameters, relative to the center of the coordinate system (optimal model and 95% confidence intervals):

East (km): 0.016 (-0.115 to -0.110)

North (km): 0.268 (0.152 to 0.425)

Depth (km): 1.7 (1.6 to 1.9)

Volume change (km^3): -0.038 (-0.043 to -0.035)

Location of Mogi source: 17.312°W, 64.432°N

(17.310°W to 17.314°W; 64.431°N to 64.433°N)

Supplementary Fig. 6 shows the marginal posterior probability distributions of the four model parameters (location in east, north, depth, and volume change). The contour plots show the density of models indicating the correlation between each parameter. The histograms along the bottom row depict the distribution of each parameter. A fairly narrow range of model parameters (95% confidence limits) is found despite a strong correlation between them.

9

2 Supplementary Discussion

During the 2011 Grímsvötn eruption the ratio $\Delta P / \Delta P_{total}$, as inferred from geodesy, shows the same variations as integrated magma flow estimated from plume height. This suggests a direct physical connection between the two. The exponential decay can be explained by coupling of the magma chamber and the eruption plume through a conduit system of fixed parameters. After emplacement of the feeder, magma flow towards the vents is approximated as flow in a pipe of equal cross-sectional area as the effective conduit. If the flow is treated as laminar[33], in a pipe with length L, then the volumetric flow rate is

$$Q = -\frac{\pi R^4}{8\eta}\frac{\Delta P}{L}$$

where η is the magma viscosity and πR^2 is the effective cross sectional area. The pressure drop over the distance of the conduit is set equal to the overpressure in the chamber. Combining the equation above with equation (3) gives the evolution of overpressure, ΔP, and magma flow rate, Q, as:

$$\Delta P(t) = \Delta P_0 e^{-t/\tau} \qquad Q(t) = Q_0 e^{-t/\tau} \qquad \tau = 8\frac{La^3}{R^4}\frac{\eta}{\mu}\left(1 + \frac{4\mu}{3k}\right)$$

where τ is a decay constant. A similar set of equations holds true even for non-laminar flow as long as magma flux is proportional to the pressure drop (then with a different set of constants). The model above can be compared to our observations. It predicts that the rate of pressure decrease and magma flow decay exponentially in the same manner. Our observations show this behavior and fit well to $\tau = 8.0$ hours (Fig. 3). The decay constant depends on a combination of six model parameters, making it difficult to estimate each independently. A direct estimate of the ratio of host rock rigidity and magma bulk modulus is possible as it relates to the ratio of volume change of a Mogi source, $\Delta V_{chamber}$, equal to $(4/3)\pi C$ [10], and the volume of magma flowing in/out of it[34,35]

10

$$\Delta V_{magma} = -\pi \left(\frac{1}{\mu} + \frac{4}{3k} \right) a^3 \Delta P$$

giving

$$\frac{\Delta V_{magma}}{\Delta V_{chamber}} = 1 + \frac{4}{3} \frac{\mu}{k} = 1 + \frac{\beta_{magma}}{\beta_{chamber}}$$

The volume ratio can also be written in terms of compressibility of the magma, β_{magma} = $1/k$, and the compressibility of the chamber, $\beta_{chamber}$ as indicated above, where $\beta_{chamber} = 3/(4\mu)$ for spherical shaped chambers[12]. The inferred cumulative DRE volume of eruptive products is ΔV_{magma} = $(270\pm70)\times10^6$ m^3 and the chamber volume change during the eruption is $(27\pm3)\times10^6$ m^3 (Table 1). The inferred β_{magma} / $\beta_{chamber}$ ratio is then 9±4. The oscillations in plume activity superimposed on the general exponential decline in magma flow can be reproduced if the model conduit parameters do not remain constant. The ash deposits suggest eruption phases dominated by magmatic fragmentation alternated with phreatomagmatic fragmentation, indicating variable access of external water to the conduit. Dynamic processes associated with magma fragmentation, causing e.g. variation in the depth of the fragmentation front in the conduit, may be responsible for modulation of magma ascent velocity in the conduit and contribute to these variations in eruption phases.

The model presented here has a feeder connecting a magma chamber to the surface, with an overall decay in the eruption rate reflecting pressure drop in the magma chamber as the eruption evolves. This model may be most applicable to simple basaltic magmatic systems that collect magma into a single chamber prior to an eruption. More complicated situation may arise in the case of two or more interacting magma bodies, or if an eruption of silicic magma is triggered by the intrusion of basalt. Similar observations as we present, of geodetic displacements and estimates of eruptive flux, at more volcanoes of different types are needed to reveal if silicic magma systems are more complicated in this respect than basaltic systems like Grímsvötn volcano.

3 Supplementary References

24. Fierstein, J. & Nathenson, M. Another look at the calculation of fallout tephra volumes. *Bull. Volcanol*. 54, 156–167 (1992).

25. Geirsson, H. *et al*. Overview of results from continuous GPS observations in Iceland from 1995 to 2010. *Jökull*, **60**, 3-22 (2011).

26. Dow, J. M., Neilan, R. E. & Rizos, C. The International GNSS Service in a changing landscape of Global Navigation Satellite Systems. *Journal of Geodesy* **83**, 191–198 (2009).

27. Houlié, N., Briole, P., Nercessian, A. & Murakami, M., Sounding the plume of the 18 August 2000 eruption of Miyakejima volcano (Japan) using GPS. *Geophys. Res. Lett.,* **32**, L05302 (2005).

28. Cervelli, P. F. *et al*. in *The 2006 Eruption of Augustine Volcano, Alaska: Geodetic constraints on magma movement and withdrawal during the 2006 eruption of Augustine volcano* (eds. Power, J. A. *et al*.) 427-452 (USGS Professional paper 1769, 2010).

29. Grapenthin, R., Freymueller, J. T. & Kaufman, A. M. Geodetic Observations during the 2009 eruption of Redoubt Volcano, Alaska, *J. Volc. Geotherm. Res*. (2012).

30. Tryggvason, E. *The N.V.I magnetoresistor tiltmeter results of observations 1977-1981* (Nordic Volcanological Institute report 8203, 1982).

31. Ferro, A. *et al*. High Precision Tilt Observationat Mt. Etna Volcano, Italy. *Acta Geophysica* **59**, 618-632 (2011).

32. Hooper, A., Segall, P. & Zebker, H. Persistent scatterer interferometric synthetic aperture radar for crustal deformation analysis, with application to Volcan Alcedo, Galapagos. *J. Geophys. Res.* **112**, B07407 (2007).

33. Jaupart, C. in *Encyclopedia of Volcanoes: Magma ascent at shallow levels* (eds Sigurdsson, H. *et al*.) 237-245 (Academic Press, San Diego, Calif 2000).

34. Johnson, D. J., Sigmundsson, F. & Delaney, P. T. Comment on ''Volume of magma accumulation or withdrawal estimated from surface uplift or subsidence, with application to the 1960 collapse of Kilauea Volcano'' by T. T. Delaney and D. F. McTigue. *Bull. Volcanol.* **61**, 491-493 (2000).

35. Rivalta, E. & Segall, P. Magma compressibility and the missing source for some dike intrusions, *Geophys. Res. Lett*., **35**, L04306 (2008)
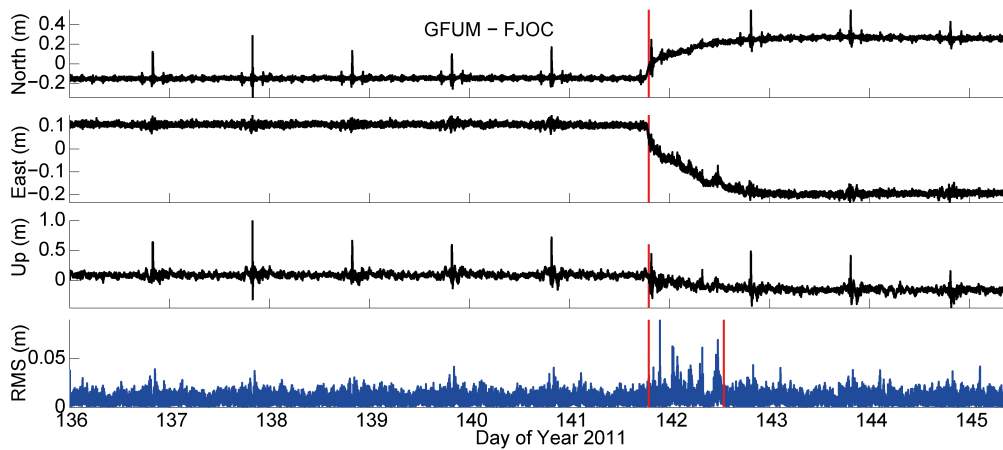
4 Supplementary Figures
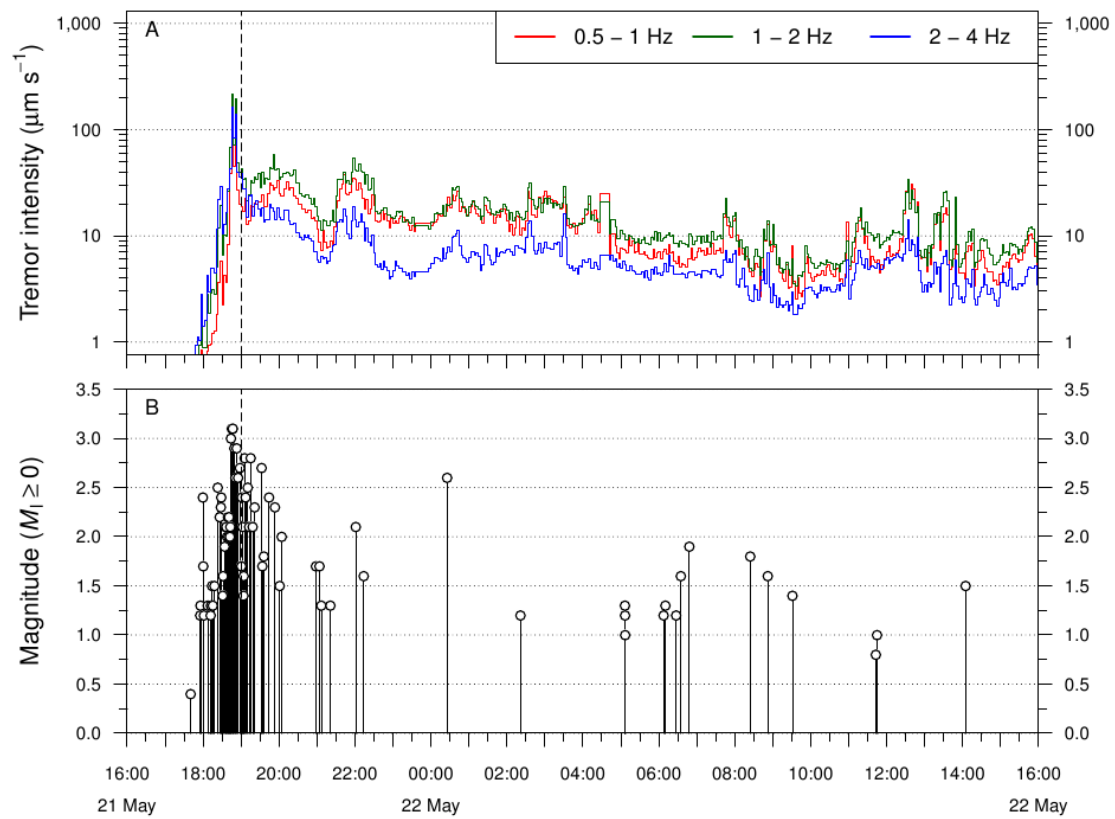
Supplementary Figure 1: Earthquakes (64.27-64.54°N, 17.5-17°W) and seismic tremor (3-minute running median) in different frequency bands, at Mt. Grímsfjall seismic station on 21-22 May, 2013.

14
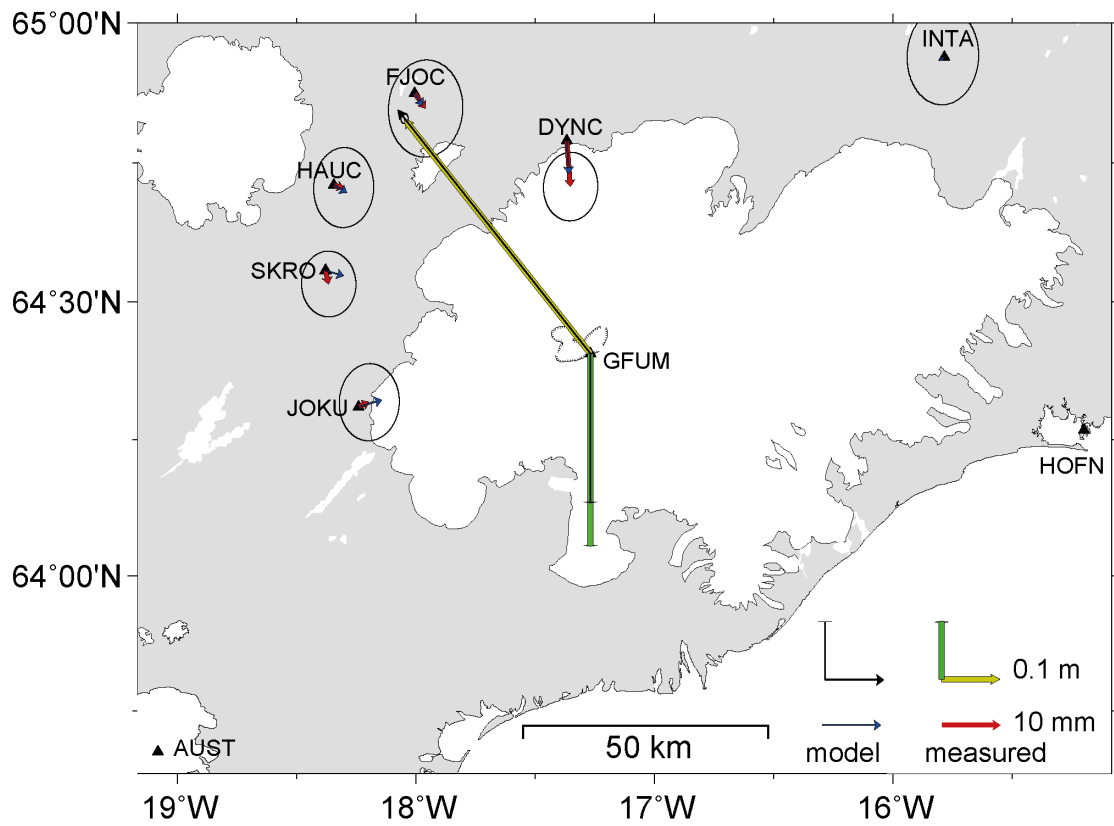
Supplementary Figure 2: Measured and modeled co-eruptive GPS displacements. Arrows (red and yellow) show co-eruptive horizontal deformation with 95% error ellipses. Bars indicate predicted (black) and measured (green) vertical motion at GFUM. Note the scale change for far-field versus GFUM displacements (1:10).

15

Supplementary Figure 3: Kinematic GPS time series of station GFUM with FJOC as base station (Fig 1, northernmost blue triangle NW of Vatnajökull) from 16-25 May 2011 prior to sidereal filtering. In the final time series we applied sidereal filtering to remove the noise that repeats every GPS day resulting from multipath effect. The lowest panel shows the misfit of the GPS solution to the data. The first red line in all panels indicates the onset of explosive activity at 19:00 on 21 May. The second red line in the lowest panel indicates 13:00 on 22 May; around this time plumes remained at or below 15 km altitude according to the radars (Fig. 1C). Note the pulsating activity in the misfit between the red lines, which indicates signal disturbance due to the plume[28] and correlates well with the plume heights given in Fig. 1.

16
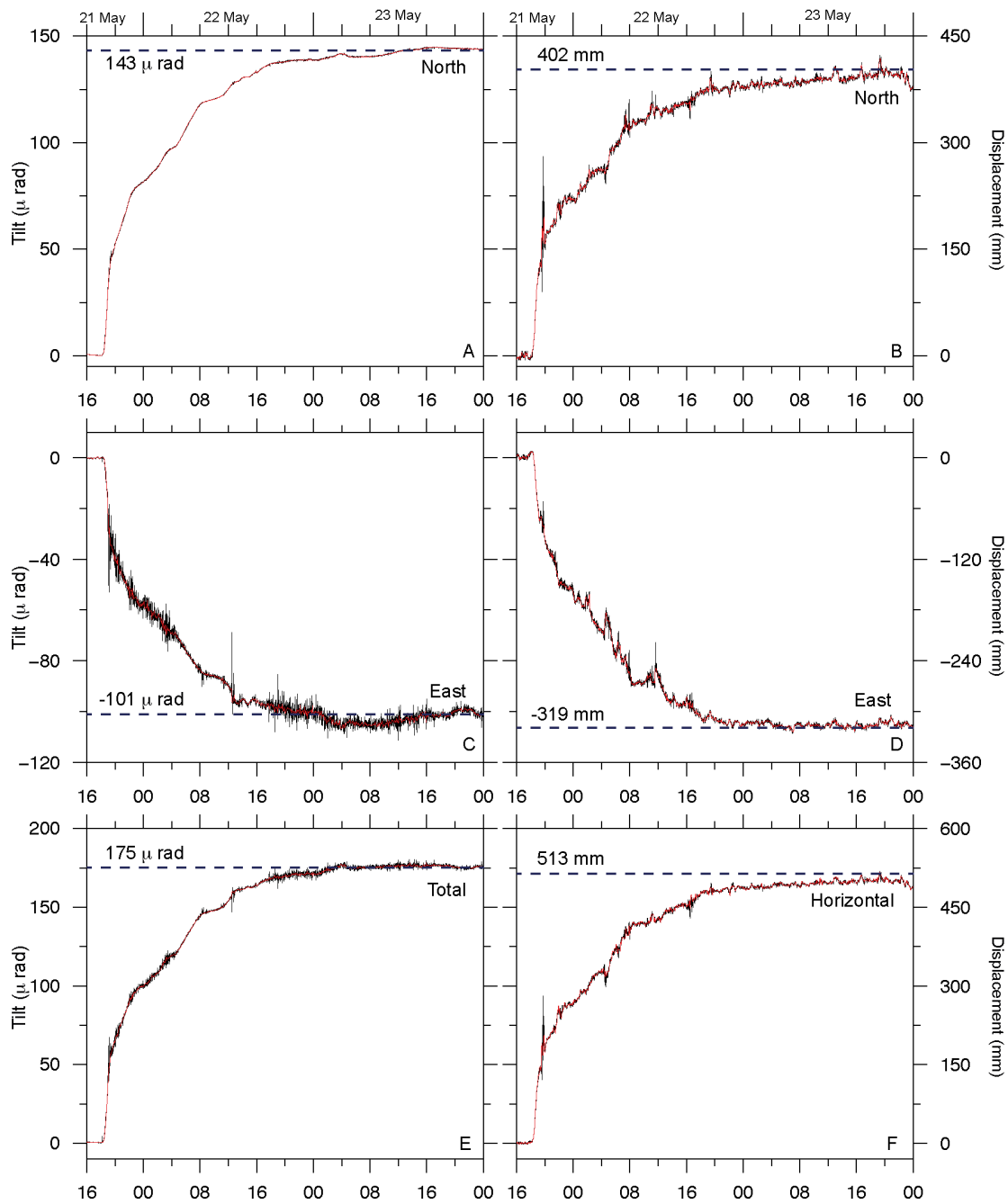
Supplementary Figure 4: Time series based on tilt and 1 Hz GPS data analyses, from 21-23 May. (**A**) North component of tilt, (**B**) North component of GPS-displacement, (**C**) East component of tilt, (**D**) East component of GPS-displacement, (**E**) Total tilt (**F**) Total horizontal displacement. Black line shows data with 1-minute filter applied, the red line has 5-minute filter applied. Hatched straight lines mark the maximum change of each component in relation to the eruption.

17
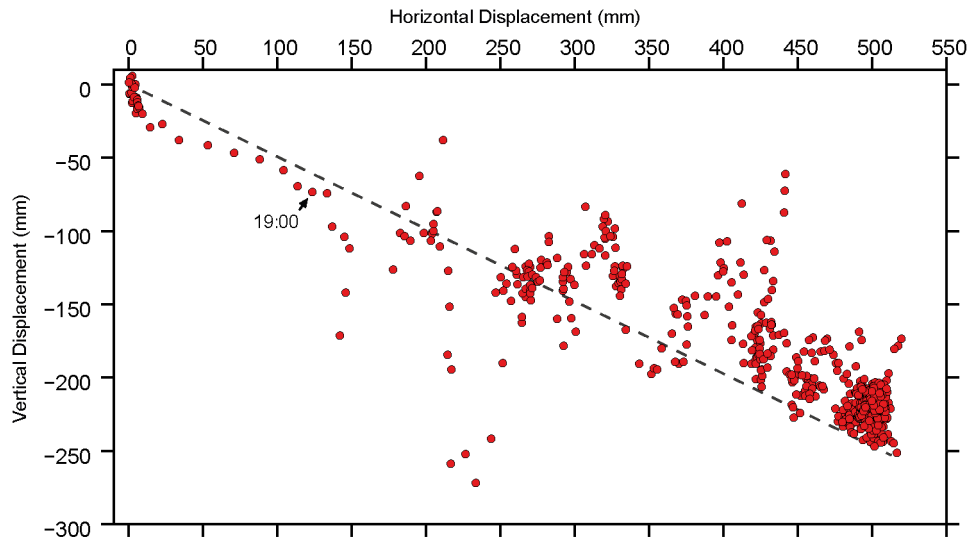
Supplementary Figure 5: 5-minute averages of total horizontal displacement (x-axis) and vertical displacement (y-axis). The line goes through (0,0) and (513, -253) with a slope of 2.03±0.09.
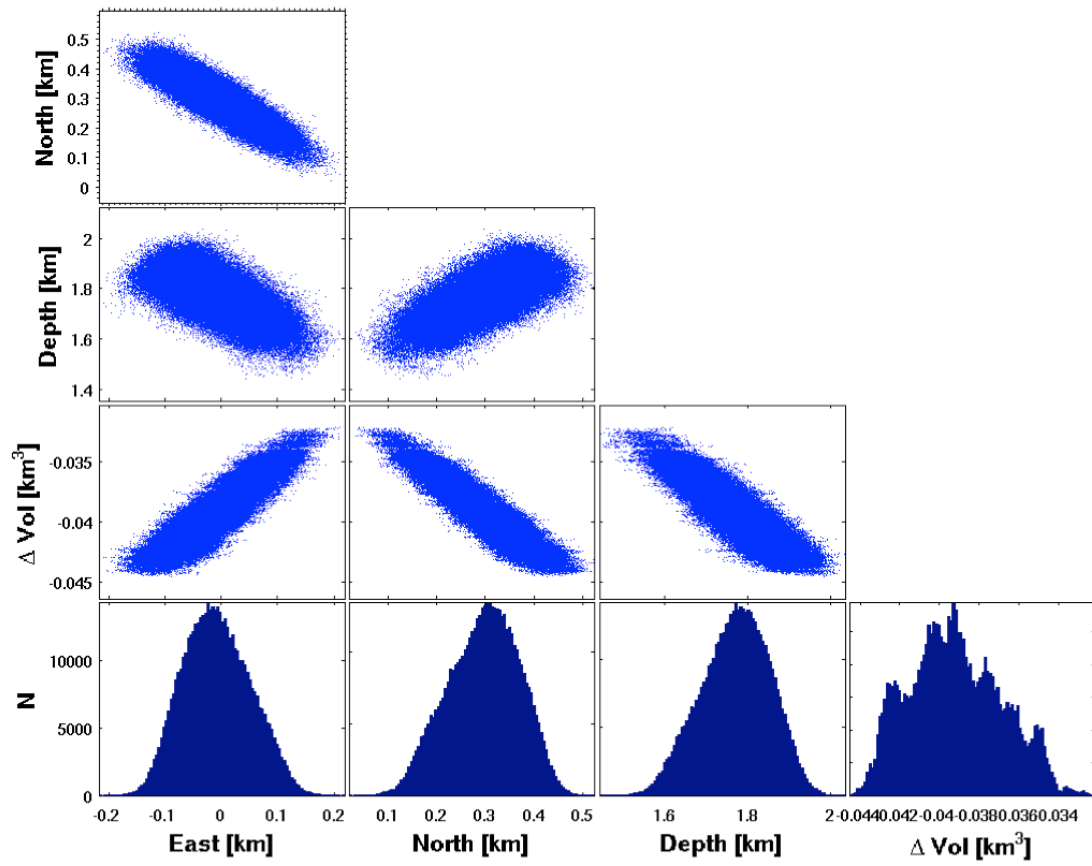
Supplementary Figure 6: Marginal posterior probability distributions of model parameters.

5 Supplementary Tables

Maximum observed deformation	GPS (mm)	Tilt (μrad)
North	402±3	143±6
East	-319±3	101±5
Direction of movement	N38.4±0.5°W	N35±2°W
Horizontal displacement (u_r), Total tilt (δ)	513±4	175±6
Vertical displacement (u_z)	-253±10	
u_r/u_z	2.03±0.09	
Percentage of change taking place prior to onset of eruption	25±1%	

Supplementary Table 1: Displacement and tilt associated with the eruption.
Displacement and tilt from onset of deformation associated with the eruption until maximum observed change on mid-day 23 May, and associated 1σ uncertainty.

	$\sigma_{tilt,x}$ (μrad)	δ_x (μrad)	T (days)	N
North-south	5.9	143	1.92	5
East-west	5.0	101	1.92	8

Supplementary Table 2: Uncertainty of tilt components. See text for explanation.